An assessment of *k–ε* and *k–l* turbulence models for a wide range of oscillatory rough bed flows

S. B. Letherman, M. A. Cotton, P. K. Stansby, C. Chen and D. Chen

ABSTRACT

The *k–ε* and *k–l* eddy viscosity turbulence models are now used extensively in environmental flow modelling. In the present work computations for oscillatory flows are examined over a broader range of experimental parameters than considered previously. Comparisons are made with field measurements and laboratory data, including new measurements reported here for the first time. It is confirmed that the bed friction velocity and mean flow profiles are, in general, adequately predicted by both models (the *k–ε* model is, however, somewhat more accurate than the *k–l* formulation). Reynolds shear stress, turbulent kinetic energy, and eddy viscosity are less well predicted, although the *k–ε* model again gives more accurate results than the *k–l* model. An attempt has been made to assess the uncertainty in the experimental data for Reynolds stress and eddy viscosity: it is found that the *k–ε* model computations for both quantities more frequently lie within the estimated uncertainty bounds. Those bounds are nonetheless wide, emphasizing the need for improved experimental resolution of rough bed flows. Such an improvement would assist in the evaluation of proposed refinements to commonly used turbulence models such as those under investigation here and, indeed, to greater reliability in the development and assessment of more sophisticated schemes.

Key words | boundary layers, oscillatory, rough bed, turbulence models

S. B. Letherman
M. A. Cotton (corresponding author)
C. Chen
D. Chen
School of Engineering,
University of Manchester,
Manchester M13 9PL,
UK
Tel (+44) 161 275 4366;
Fax (+44) 161 275 4346;
E-mail: *mark.cotton@man.ac.uk*

P. K. Stansby
Department of Civil and Construction Engineering,
UMIST,
Manchester M60 1QD,
UK

INTRODUCTION

Oscillatory boundary layers in the natural environment occur in estuaries and coastal regions due to tidal flows and short-period wind waves. The bed is generally hydraulically rough and, at high Reynolds numbers, the boundary layer may be characterized by the parameter a/k_s provided that $\delta/h<1$, where a is the amplitude of particle motion outside the boundary layer, k_s is the Nikuradse roughness height, h is the water depth, and δ is the unbounded boundary layer thickness (defined, for example, by Jensen *et al*. 1989). There have been several numerical investigations based upon *k–ε* and *k–l* eddy viscosity turbulence models (k is the turbulent kinetic energy, ε is the rate of viscous dissipation of k, and l is a turbulence length scale). The application of both *k–l* (Justesen 1991; Sajjadi & Waywell 1998) and *k–ε* models (Justesen 1991; Baumert & Radach 1992; Stansby 1997; Sajjadi & Waywell 1998; Thais *et al*. 1999) to rough bed boundary layers has indicated that a broadly satisfactory performance is achieved. It should, however, be noted that predictions of eddy viscosity have not been assessed, and it is the eddy viscosity that determines the mixing of solute and sediment (at least within an assumed Fickian framework). Clearly, such predictive capability is of fundamental importance within general environmental flow and material transport modelling. In this paper we report 1D-vertical numerical simulations using the above turbulence models for various laboratory and field conditions covering a wide range of a/k_s (from 86 to 3.6×10^6) and k_s/h (from 10^{-4} to 10^{-1}). The lower bound on the a/k_s range is close to the limit of applicability of the present modelling approach because of assumptions implicit in the associated 'wall functions' (which provide the bed boundary

Table 1 | Summary of the experimental data

Case	T (s)	h (m)	U_0 (m/s)	a (m)	k_s (m)	a/k_s	k_s/h	δ/h	k_s^+	Re
Jade	44,700	20.0	1.00	7114	0.002	3.6×10^6	0.0001	2.1	69	7.1×10^9
Elbe	44,700	5.1	1.10	7826	0.02	3.9×10^5	0.0039	13.6	820	8.6×10^9
JSF13	9.72	0.14	2.00	3.09	0.00084	3700	0.006	0.46	84	6.2×10^6
JSF12	9.72	0.14	1.02	1.58	0.00084	1880	0.006	0.26	44	1.6×10^6
UKCRF	180	0.48	0.10	2.86	0.02	140	0.042	0.22	240	2.9×10^5
UMTF	60	0.10	0.09	0.86	0.01	86	0.1	0.35	90	7.7×10^4

conditions on the momentum and turbulence transport equations); the upper value of k_s/h represents rather shallow flow which is nonetheless of practical importance. δ/h varies from approximately 0.2 to values in excess of 1; for $\delta/h>1$ the boundary layer interacts with the free surface and in such cases the particle amplitude, a, is defined at the surface.

The sources of experimental data and the defining parameters of the various cases are listed in Table 1. The Jade estuary data are given by McLean (1983) and the Elbe estuary data by Schröder (1987). The cases 'JSF13' and 'JSF12' refer to the data of Jensen *et al*. (1989) obtained in an oscillating water tunnel (Justesen (1991) has previously reported model comparisons with the JSF data). 'UKCRF' denotes previously unpublished data from the work of Lloyd *et al*. (1997) undertaken at the UK Coastal Research Facility located at HR Wallingford; 'UMTF' refers to further unpublished data from the smaller tidal flume at the University of Manchester. The values of k_s quoted in Table 1 for the Jade and the Elbe are taken from Baumert & Radach (1992); the JSF values are supplied by the original authors, and in the UKCRF and UMTF cases k_s is taken as $2d$ (where d is the grain diameter).

Bed friction velocity is compared with the JSF, UKCRF, and UMTF data. Phase-averaged (or 'mean') velocity profiles are compared with the UKCRF and UMTF data. The UKCRF and UMTF measurements extend the a/k_s and k_s/h parameter range of the JSF experiments (reducing a/k_s and increasing k_s/h). Computed Reynolds shear stress is compared with data for the Jade and Elbe; the Reynolds stress and turbulent kinetic energy variations are examined over a range of depths for the JSF and UMTF cases, and eddy viscosities are estimated for the JSF data. The Jade and Elbe data have previously been modelled by Baumert & Radach (1992) and Stansby (1997) using the k–ε model: it is Stansby's scheme that is adopted here (the 1D version in present use is based upon a general 3D solver and incorporates a parabolic mesh generator to give high flow definition at the bed). Sajjadi & Waywell (1998) have applied eddy viscosity and also Reynolds stress transport models to these cases. Their k–ε model results were similar to those of Baumert & Radach (1992) and all the models tested were in good agreement with the data.

An important aspect of the present study is an assessment of the accuracy with which the k–ε and k–l models compute eddy viscosity. Under experimental conditions it is necessary to employ many oscillation cycles (at least 50) in order to obtain statistically meaningful estimates of this quantity (Sleath 1987; Jensen *et al*. 1989). In relation to the experimental work discussed above, data of this quality are available only for the JSF and UMTF cases. An attempt has been made here to quantify the uncertainty in the experimental estimates for eddy viscosity in order to permit a realistic evaluation of model capabilities. Some preliminary findings in this area were presented by Letherman (1999).

While there have been numerous studies of smooth bed flows, the present work is concerned only with

hydraulically rough flows. Significant earlier experimental contributions to the understanding of rough bed flows have been made by Jonsson & Carlsen (1976) and Sleath (1987); however, their defining parameters are largely covered by the JSF and UMTF cases (although Sleath did examine some extremely rough beds with correspondingly small a/k_s values: in fact, the smallest values of a/k_s studied by Sleath are beyond the limitations of the present computational framework).

MATHEMATICAL FORMULATION

The governing equations are written in a phase-averaged 1D-vertical formulation such that all flow variables, apart from the pressure gradient, are functions of the vertical coordinate, z, and time or phase position. (In all cases z is measured from a datum set at $0.2d$ below the top of the roughness elements, i.e. $z = z' - 0.8d$, where z' is measured from the base of the grains.) The horizontal pressure gradient is a function of time only. The phase-averaged horizontal velocity, U, is determined from the unsteady momentum equation:

$$\frac{\partial U}{\partial t} = -\frac{1}{\rho}\frac{\partial p}{\partial x} + \frac{\partial}{\partial z}\left(\nu\frac{\partial U}{\partial z} - \langle uw\rangle\right) \tag{1}$$

In Equation (1) t is time, ρ is density, p is pressure, ν is molecular kinematic viscosity, and $-\langle uw\rangle$ represents the phase-averaged Reynolds shear stress (with u and w the horizontal and vertical fluctuating velocities, respectively). The introduction of an eddy viscosity, ν_t, relates the Reynolds stress to the vertical velocity gradient:

$$-\langle uw\rangle = \nu_t\frac{\partial U}{\partial z} \tag{2}$$

The *k–ε* model

In the k–ε eddy viscosity model ν_t is determined as a function of the phase-averaged turbulent kinetic energy, k, and the rate of viscous dissipation of k, denoted by ε:

$$\nu_t = C_\mu\frac{k^2}{\varepsilon} \tag{3}$$

The model incorporates differential equations for the determination of both k and ε. In a physical sense, therefore, transport (unsteady and diffusive) effects influence the evolution of both turbulence quantities through a cycle. The k- and ε-transport equations are

$$\frac{\partial k}{\partial t} = \nu_t\left(\frac{\partial U}{\partial z}\right)^2 + \frac{\partial}{\partial z}\left[\left(\nu + \frac{\nu_t}{\sigma_k}\right)\frac{\partial k}{\partial z}\right] - \varepsilon \tag{4}$$

$$\frac{\partial \varepsilon}{\partial t} = C_{\varepsilon 1}\frac{\varepsilon}{k}\nu_t\left(\frac{\partial U}{\partial z}\right)^2 + \frac{\partial}{\partial z}\left[\left(\nu + \frac{\nu_t}{\sigma_\varepsilon}\right)\frac{\partial \varepsilon}{\partial z}\right] - C_{\varepsilon 2}\frac{\varepsilon^2}{k} \tag{5}$$

The constants appearing in Equations (3)–(5) are assigned the standard values $C_\mu = 0.09$, $\sigma_k = 1.0$, $\sigma_\varepsilon = 1.3$, $C_{\varepsilon 1} = 1.44$, and $C_{\varepsilon 2} = 1.92$ (Rodi 1993).

The *k–l* model

A somewhat simpler means of determining the eddy viscosity is available in the form of the k–l turbulence model. On dimensional grounds the length scale of the energy-containing turbulent eddies is obtained as being of the order of $k^{3/2}/\varepsilon$. Taking the constant of proportionality as $C_\mu^{3/4}$ and equating l to the Prandtl mixing length:

$$\ell = C_\mu^{3/4}\frac{k^{3/2}}{\varepsilon} = \varkappa z \tag{6}$$

where $\varkappa$ is the von Kármán constant (taken as 0.4 throughout the present study). It follows from Equations (3) and (6) that ν_t may be expressed in terms of k and z only:

$$\nu_t = \varkappa C_\mu^{1/4}k^{1/2}z \tag{7}$$

ε appearing as the sink term of Equation (4) is obtained from Equation (6). In a strictly mathematical sense, therefore, the need for an ε-transport equation is obviated, although viewed more physically this means that non-equilibrium effects on the length-determining scale are neglected. The constants of the standard k–l model are assigned the values $C_\mu = 0.08$ and $\sigma_k = 1.0$ (Justesen 1991;

Rodi 1993). Sensitivity to the value of C_μ adopted in the k–l model is examined below (cf. the k–ε model value quoted above) and, in relation to the more advanced scheme, further sensitivity tests are made on the value of the σ_ε, the turbulent Prandtl number governing the diffusion of the dissipation rate variable.

Remarks concerning the k–ϵ and k–l models

The preceding discussion highlights the relative inadaptability of the k–l scheme, in that a prescribed turbulence length scale, l, forms an element of the model. Thus, irrespective of changing mean flow and turbulence conditions, l in Equation (6) is taken to increase linearly with z, the vertical coordinate. (Other prescriptions of l are possible, for example a 'cut-off' could be applied to the linear variation, but nonetheless the basic assumption of a fixed distribution of the length scale remains.) In the k–ε model, in contrast, the effective length scale ($k^{3/2}/\varepsilon$) varies both spatially and temporally in response to changes in the two turbulence variables as determined from the solution of Equations (4) and (5).

Considering next the more detailed formulation of the k–ε model, the present work seeks to examine the standard form of the model against the equivalent k–l standard. It is noted, however, that various refinements to the standard model have been proposed. In relation to C_μ, the constant appearing in the constitutive equation of the model (Equation (3)), Celik & Rodi (1984) have advanced modifications to account for both free surface and near-bed effects (see also Nezu & Nakagawa 1993); Cotton & Ismael (1998) consider the effect of high strain rates upon the effective value of C_μ. The work of Sajjadi & Waywell (1998) examining advanced Reynolds stress transport models was mentioned briefly in the Introduction: while those models showed no particular advantage over k–ε and k–l schemes in application to the field data of McLean (1983) and Schröder (1987), the same authors (Sajjadi & Waywell 1997) found a stress transport model to be more accurate than a k–l formulation in comparison with the laboratory data of Sumer *et al.* (1987) and Jensen *et al.* (1989). It remains the task of the present study to carefully evaluate established k–ε and k–l models against a range of experimental data for rough bed oscillatory flows.

Boundary conditions

The lower boundary condition on velocity is given by the semi-logarithmic velocity profile (or 'law-of-the-wall') for fully rough turbulent boundary layers (Schlichting 1979, p 619):

$$U_1^+ = \frac{|U_1|}{U_\tau} = \frac{1}{\kappa} \ln\left(\frac{z_1}{k_s}\right) + 8.5 \tag{8}$$

where the friction velocity, $U_\tau = (\,|\,\tau_b\,|\,/\rho)^{1/2}$ and τ_b is the bed shear stress. The subscript 1 denotes the first velocity node above the bed. Conventional bed-adjacent boundary conditions on k and ε are applied:

$$k_{1(t)} = \frac{U_\tau^2}{\sqrt{C_\mu}} \tag{9}$$

$$\varepsilon_{1(t)} = \frac{U_\tau^3}{\varkappa z_{1(t)}} \tag{10}$$

where the subscript 1(t) denotes the first turbulence node above the bed. The equilibrium assumptions underlying Equations (9) and (10) are discussed by Cotton & Stansby (2000). At the upper boundary the shear stress is zero and hence the velocity gradient $\partial U/\partial z = 0$. Upper boundary conditions on k and ε at the surface are also supplied using the zero gradient conditions $\partial k/\partial z = \partial \varepsilon/\partial z = 0$ (Rodi 1993).

Input parameters

Two versions of the 1D-vertical computer code were used in the present study. The principal difference between the two lies in the input parameter for solution of the momentum equation, Equation (1). In cases where the tidal set-up may be specified (the Jade and the Elbe) the driving horizontal pressure gradient, $-\partial p/\partial x$, is obtained directly as a function of time. In cases JSF13 and JSF12 the controlled experimental variable was the freestream velocity, U_∞, and the boundary layer pressure gradient may be determined from the inviscid Euler equation:

$$\frac{dU_\infty}{dt} = -\frac{1}{\rho}\frac{\partial p}{\partial x} \tag{11}$$

In the larger-scale UKCRF and UMTF experiments, however, volumetric flow rate or bulk velocity was the controlled quantity. In simulating these cases an integral continuity constraint in which bulk velocity is prescribed as a function of time is added to the equation set:

$$U_b(t) = \frac{1}{h}\int_0^h U(z,t)\,dz \tag{12}$$

Numerical procedures

The present numerical procedures are described in detail by Stansby (1997) for the parent 3D algorithm. Here we limit discussion to a brief treatment of the spatial flow discretization and method of time advancement adopted in the 1D program.

The nodes for velocity, U, and the turbulence variables, k and ε, are staggered in the vertical direction. Steep gradients of flow variables occur in the near-bed region and therefore a parabolic mesh spacing is employed to give high resolution in the lower part of the domain. Following Cotton & Stansby (2000) an attempt was made to use 100 velocity nodes and also to position the first velocity node to satisfy the dual criteria:

$$30 \le z^+_{1,\max} \le 100 \tag{13}$$

$$0.03 \le \frac{z_1}{k_s} \le 0.1 \tag{14}$$

The first criterion (in which $z^+_{1,\max} = z_1, U_{\tau,\max}/\nu$) was satisfied without exception in the present work. It proved not to be possible, however, to use 100 nodes and to simultaneously satisfy Equation (14) for all the cases examined. To cite two examples, in simulating the JSF experiments 100 nodes were used and Equation (14) was satisfied; making comparison with the UMTF data, in contrast, only 10 velocity nodes could be used while maintaining z_1/k_s within the specified range. In fact, the maximum value of z_1/k_s did frequently exceed 0.1: in a third example (the Jade) a value $z_1/k_s = 1.8$ was used in conjunction with 100 nodes.

The solution is marched in time using an implicit solution algorithm. Thus, for the momentum equation (Equation (1)) the velocity, U, which appears in both the unsteady and shear stress gradient terms, is evaluated at a new time step using a specified value of pressure gradient (or bulk velocity) and the 'old' eddy viscosity distribution (Equations (2) and (3)). In the case of the turbulent kinetic energy, k (Equation (4)), a similar procedure is adopted and the net production-minus-dissipation generation rate is treated explicitly as a source term. A slightly different technique is applied in the treatment of the ε-equation (Equation (5)): here, the production-minus-destruction source term is handled in a semi-implicit manner (Stansby 1997). The numerical parameters of the time advancement scheme varied between the different experimental test cases: in the simulation of the experiments of Jensen *et al*. (1989), 600 time steps per cycle were employed and the computer program was run for 5 cycles; the corresponding figures in comparison with the UMTF data were 10^4 time steps and 10 cycles of oscillation.

Sensitivity tests

The sensitivity of the computed results to both physical and numerical parameters was investigated in the course of the study. The physical tests that relate to turbulence model constants have been indicated above and will be discussed under Results. An extensive series of numerical sensitivity tests was conducted on simulations of the two JSF cases and the UMTF data: an assessment of sensitivity to changes in a given parameter was made by reference to the value of the wave friction factor, $f_w = \tau_{b,\max}/(\frac{1}{2}\rho U^2_{\infty,\max})$. The largest change in f_w (-11%) was recorded when $z^+_{1,\max}$ was increased from approximately 40 to 90 while simultaneously the number of spatial nodes was halved. At least in respect of the wave friction factor, this figure must be seen as a measure of the uncertainty associated with a conventional implementation of rough bed boundary conditions. (Some further discussion of numerical sensitivity issues may be found in Cotton & Stansby (2000).)

RESULTS

The k–ε and k–l models are compared below against the six experimental cases detailed in Table 1. In addition to those variables defined previously, Table 1 quotes the period of oscillation, T, the amplitude of the freestream or surface velocity, $U_0(\equiv U_{\infty,\max})$, $k_s^+ = k_s U_{\tau,\max}/\nu$, and Reynolds number, $\mathrm{Re} = U_0 a/\nu$. Experimental values for $U_{\tau,\max}$ are used in the JSF, UKCRF, and UMTF cases; for the Jade and Elbe an approximate value is obtained from a correlation supplied by Nielsen (1992, p 25):

$$f_w \equiv \frac{U_{\tau,max}^2}{\frac{1}{2}U_0^2} = \exp\left(5.5\left(\frac{a}{k_s}\right)^{-0.2} - 6.3\right) \tag{15}$$

The particle amplitude, a, is calculated as $a = U_0/(2\pi/T)$ and the boundary layer thickness, δ is estimated using a formula quoted by Fredsøe & Deigaard (1992, p 25):

$$\frac{\delta}{k_s} = 0.09\left(\frac{a}{k_s}\right)^{0.82} \tag{16}$$

The role played by the timescale of the energy-containing turbulence, k/ε, is considered in relation to the Jade and Elbe data. Estimates of experimental uncertainty are made in the course of comparisons with the JSF13 and UMTF data. Case JSF13 is also used in examining sensitivity to turbulence model constants. The comparisons with data are made primarily in terms of the variation over a cycle of various flow parameters at given elevations; in order to supplement this form of presentation, vertical flow profiles are also considered in the UKCRF and UMTF cases.

The Jade

In the first of two sets of comparisons against field data, we consider the work of McLean (1983) who made measurements over 30 (half) tidal cycles of the Jade estuary. Orthogonally-mounted mechanical current meters were used to obtain a time record of the three instantaneous velocity components. Figures 1(a) and 1(b) show the phase-averaged velocity and Reynolds shear stress at an elevation of 2.14 m ($z/h = 0.11$) above the bed. ($\delta/h = 2.1$ for this case, Table 1, and hence $z/\delta = 0.05$. The values of z/h and z/δ indicate that the data pertain to the lower region of the boundary layer, although since δ is greater than h for this flow the numerical value of the boundary layer thickness is only notional.) There is considerable scatter in the measurements, and since there is no reference phase position only magnitudes may be compared. A tidal set-up (maximum surface slope) of 2×10^{-5} was assumed (Baumert & Radach 1992). It is seen that both the k–ε and k–l models compute the velocity variation accurately; the turbulence model results show somewhat higher values of the Reynolds stress in the accelerating quarter cycle, particularly when using the k–l model. Figure 1(b) shows that Reynolds stress as returned by the k–ε model lags the k–l variation at the start of the cycle: this finding is to be repeated in comparisons with other

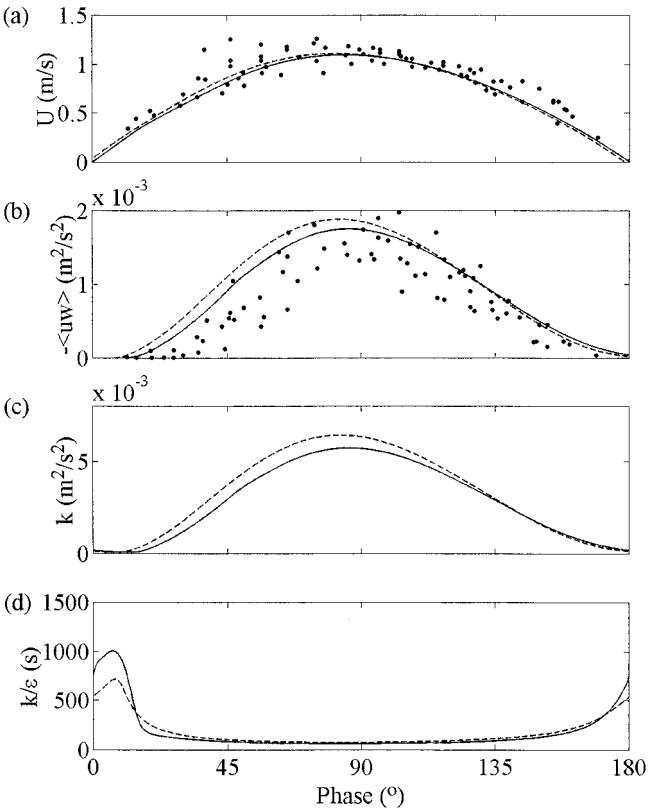

Figure 1 | Cyclic variations in the Jade estuary at 2.14 m above the bed. (a) Velocity, (b) Reynolds stress, (c) turbulent kinetic energy, (d) turbulence timescale. •Data of McLean (1983), —— k–ϵ model, – – – k–l model.

sets of data and is attributable to the inclusion of a transport, or rate, equation for ε in the former model.

Figures 1(a) and 1(b) serve largely to confirm the findings of Baumert & Radach (1992) and Sajjadi & Waywell (1998). It is interesting, however, to proceed to examine the cyclic variation of turbulent kinetic energy and the turbulence timescale. In relation to the turbulent kinetic energy, Figure 1(c) shows that both models produce a variation of k that lags the velocity by approximately 10°, or 1240 s, at the start of the cycle (and the k–ε model again lags the k–l scheme). At the maximum flow rate the lag reduces to approximately 2° (250 s). Comparison of these values with the turbulence time scales shown in Figure 1(d) reveals, as might be anticipated, that the lags are of the same order as the turbulence timescale (k/ε peaks at 700–1000 s near the start of the cycle and reduces to approximately 100 s around the maximum flow rate).

The Elbe

Subsequent to McLean's work, Schröder (1987) employed an acoustic Doppler technique to measure instantaneous velocities in the Elbe estuary. The data were recorded over 3 cycles of oscillation at an elevation of 1.9 m (corresponding to $z/h = 0.37$; for this case a value $z/\delta = 0.03$ is obtained, however, the notional boundary layer thickness exceeds the actual water depth by a factor of 14). The tidal set-up was taken as 5×10^{-5} (again following Baumert & Radach (1992)). Figures 2(a)–(c) show Schröder's data and the present computational results for velocity, Reynolds stress, and turbulent kinetic energy. It is seen that both models compute values of the Reynolds stress over the maximum flow phase interval that are more than twice as large as the measured levels. Agreement between the data and calculations for velocity and turbulent kinetic energy is, however, generally satisfactory. The turbulence models show that the 'structural ratio' $-\langle uw \rangle / k$ maintains a near-equilibrium value of approximately 0.3, in line with expectations for a slowly varying flow, and it would consequently appear that experimental effects have produced unduly low values of the Reynolds stress. (To our knowledge there is no independent model validation available, as neither Baumert & Radach (1992) nor Sajjadi & Waywell (1998) include plots of the Reynolds stress.) The turbulence timescales shown in Figure 2(d) exhibit cyclic variations similar to those observed for the Jade. It is notable, however, that there is less difference between the k–ε and k–l model results (a feature that is also apparent in Figures 2(a)–(c)). Once again, there is a clear correspondence between the energy-containing turbulence timescale and the lag of the turbulent kinetic energy behind the velocity variation.

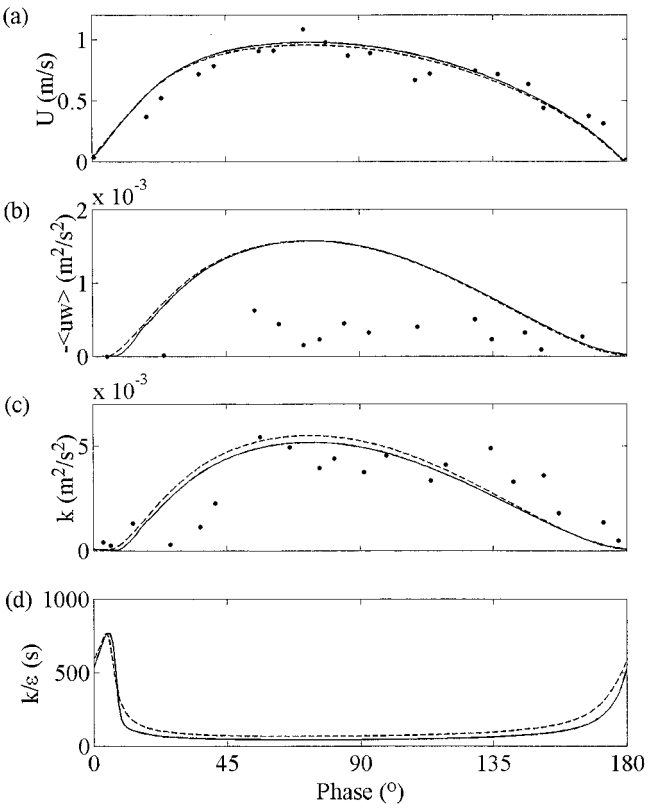

Figure 2 | Cyclic variations in the Elbe estuary at 1.9 m above the bed. (a) Velocity, (b) Reynolds stress, (c) turbulent kinetic energy, (d) turbulence timescale. •Data of Schröder (1987), —— k–ϵ model, – – – k–l model.

JSF13 and JSF12

Jensen *et al.* (1989) employed laser Doppler anemometry (LDA) to make phase-averaged mean flow and turbulence measurements in a laboratory-scale water tunnel. In addition, hot film probe measurements of the bed shear stress were reported. The two cases considered here are

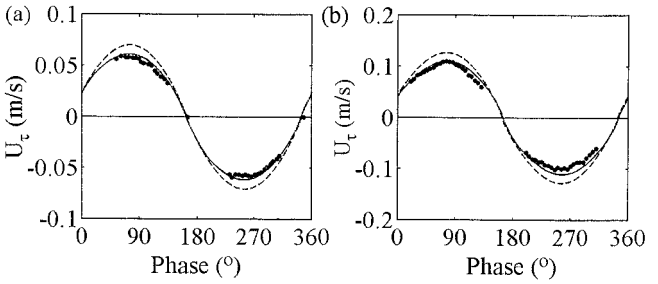

Figure 3 | Cyclic variation of friction velocity in comparison with the data of Jensen *et al*. (1989). (a) Case JSF12, (b) Case JSF13. •Data, —— *k–ε* model, – – – *k–l* model.

detailed in Table 1: JSF13 is at a sufficiently high Reynolds number (for the relative roughness of the bed) that the case may be considered as 'fully rough' ($k_s^+ = 84$); in contrast, JSF12 occupies a transitional rough-to-smooth regime with $k_s^+ = 44$. The results of the present tests of turbulence model sensitivity (for which JSF13 has been adopted as the principal test case) are reported following the presentation of results obtained using the standard *k–ε* and *k–l* models.

Experimental measurements of the bed friction velocity are shown together with the present turbulence model calculations in Figure 3. In both cases (JSF12, Figure 3(a) and JSF13, Figure 3(b)) it is seen that the *k–ε* model performs well, although the *k–l* model yields values for this practically important quantity that are 15–20% above the data. The maximum values of the friction velocity found experimentally (and computed using the *k–ε* model) are in good agreement with Equation (15).

Figure 4 depicts Reynolds shear stress data obtained by Jensen *et al*. (1989) at five different elevations in test JSF13. The plots show the variation of $-\langle uw \rangle$ over half a cycle of oscillation and it is immediately clear that there is considerable scatter in the measurements. Using a method described by Letherman (1999), a continuous polynomial of order 5, $\varphi_{\text{poly}}(\omega t)$, was first fitted to the Reynolds stress flow record at each elevation. An overall root mean square measure of uncertainty for a given elevation, $\pm \Delta\varphi$, was then evaluated as

$$\Delta\varphi = \left[\frac{1}{n} \sum_{i=1}^{n} (\varphi_{\text{data},i} - \varphi_{\text{poly},i})^2 \right]^{1/2} \tag{17}$$

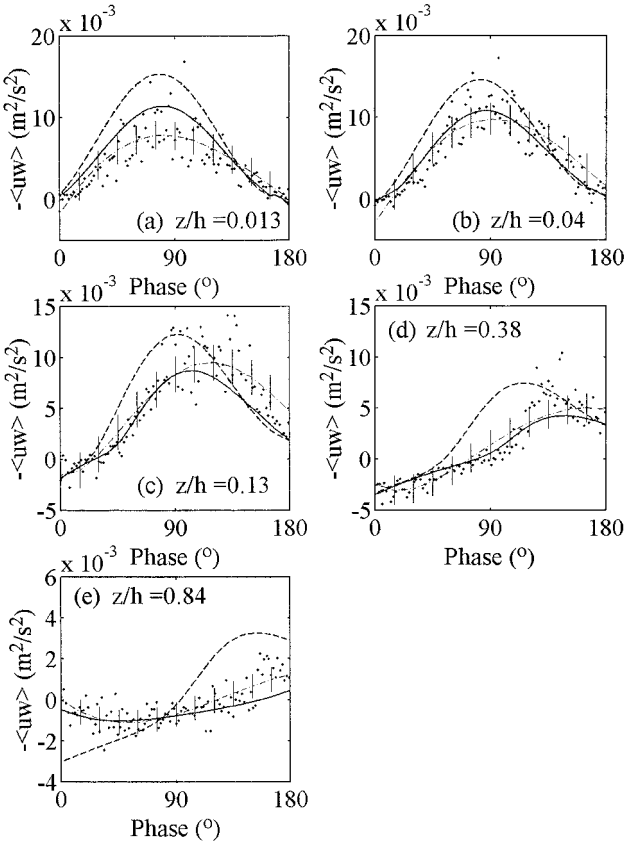

Figure 4 | Cyclic variation of Reynolds stress in comparison with Case 13 of Jensen *et al*. (1989). •Data, —— *k–ε* model, – – – *k–l* model, – · – polynomial fit to data. The vertical lines give a measure of the uncertainty in the fit to data.

where the summation extends over the n discrete measurements that constitute the flow record at the given elevation. In Figure 4 the polynomial fit to the data is shown as a chain-broken line onto which the vertical uncertainty bands are superimposed at regular intervals. It is found that 70% of the original data points fall within the uncertainty range. Figures 4(a)–(e) show that the *k–ε* model is considerably more successful than the *k–l* scheme in capturing the experimental variation of Reynolds stress. Nonetheless, the agreement obtained using the *k–ε* model is not exact: for example, the model over-predicts the Reynolds stress very close to the bed (Figure 4(a); $z/h = 0.013$ and $z/\delta = 0.03$), but under-predicts it over part of the cycle at $z/h = 0.13$ (or $z/\delta = 0.28$), Figure 4(c). In phase terms the *k–ε* model

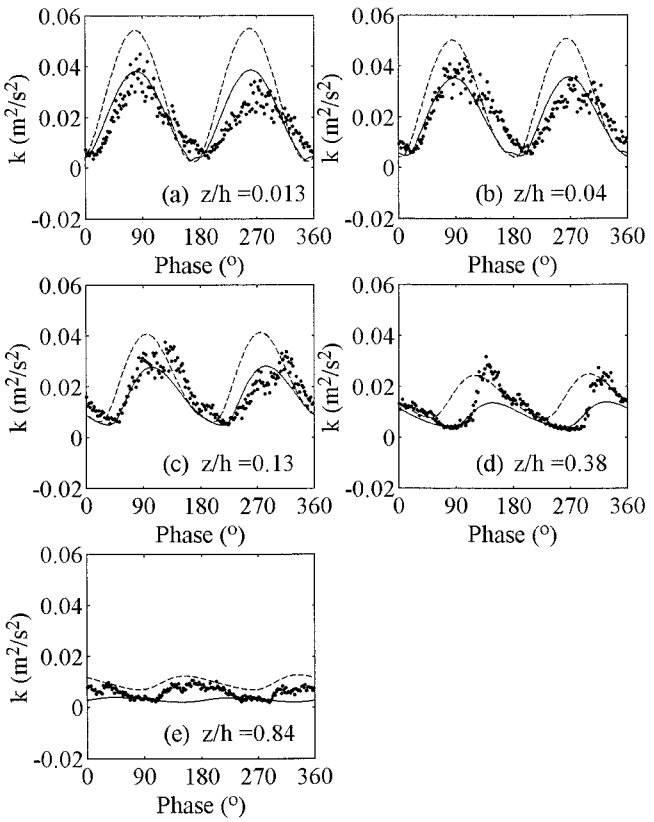

Figure 5 | Cyclic variation of turbulent kinetic energy in comparison with Case 13 of Jensen *et al*. (1989). •Data, —— *k*–ϵ model, – – – *k*–*l* model. The experimental data for k are approximated by $k' = 1.3(\langle u^2 \rangle + \langle w^2 \rangle)/2$.

is generally close to the data, although a degree of discrepancy is again apparent in Figure 4(c).

Comparison is made in Figure 5 with the turbulent kinetic energy data of JSF13. In representing the data it should be noted that turbulent kinetic energy is correctly defined as $k = \frac{1}{2}(\langle u^2 \rangle + \langle v^2 \rangle + \langle w^2 \rangle)$; however, Jensen *et al*. (1989) did not measure the spanwise component of velocity, v. Svendsen (1987) advanced a two-component approximation to the turbulent kinetic energy, viz. $k' = 1.3(\langle u^2 \rangle + \langle w^2 \rangle)/2$. The approximation was tested in the course of the present study and found to be of acceptable accuracy. The experimental points on Figure 5 therefore represent k' rather than k. Phase-averaged data plotted over a cycle show that the reverse-flow maximum in k' is always of smaller magnitude than the forward-flow value, indicating that there is some incomplete reciprocation of the flow in the experiment. Despite this observation and also the uncertainty introduced in the comparisons by the experimental approximation to k, Figures 5(a) and (b) for $z/\delta = 0.03$ and 0.09 reveal that the k–ε model captures the data well in the bed-adjacent region. In the same region the k–l model consistently over-predicts the level of k (as found in the results for Reynolds stress). At $z/\delta = 0.28$ (Figure 5(c)) there is evidence that the k–ε model under-predicts the turbulent kinetic energy data. Figures 5(d) and (e), respectively for $z/\delta = 0.83$ and 1.8, show the turbulent kinetic energy variation across the outer flow. At these elevations the k–ε model returns somewhat low levels of turbulent kinetic energy. While the k–l model is in better agreement with the measured magnitude of turbulent kinetic energy in the outer boundary layer, a distinct phase lead (of approximately 20°) is evident with respect to data. The lag of the k–ε model results behind those of the k–l model in both Figures 4 and 5 confirms the remarks made above in connection with the Jade comparisons.

The variation of eddy viscosity, ν_t, over the first half cycle is shown in Figure 6. Rearrangement of Equation (2) yields $\nu_t = -\langle uw \rangle / \partial U / \partial z$: to obtain experimental values for eddy viscosity the individual points of the Reynolds stress record of Figure 4 were divided by corresponding values of the velocity gradient derived from spatially interpolated velocity data. Values for ν_t at phase positions close to flow reversal (0°, 15°, and 180°) are omitted because of the effect of very small velocity gradients in greatly amplifying Reynolds stress uncertainties in the expression for eddy viscosity. (Note in this connection that the uncertainty bands shown in Figure 6 are associated solely with the previously evaluated uncertainties in Reynolds stress; no allowance has been made for uncertainty in the velocity gradient.) Close to the bed, examination of Figure 6(a) reveals that the k–ε model captures the data fairly satisfactorily. In contrast, the k–l variation of eddy viscosity shown in Figure 6(a) generally lies well outside the experimental uncertainty bands. It is seen in Figures 6(b)–(e) that there are portions of the half-cycle where both models yield values of ν_t beyond the limits of the estimated experimental uncertainty. Nonetheless, at least in Figures 6(b)

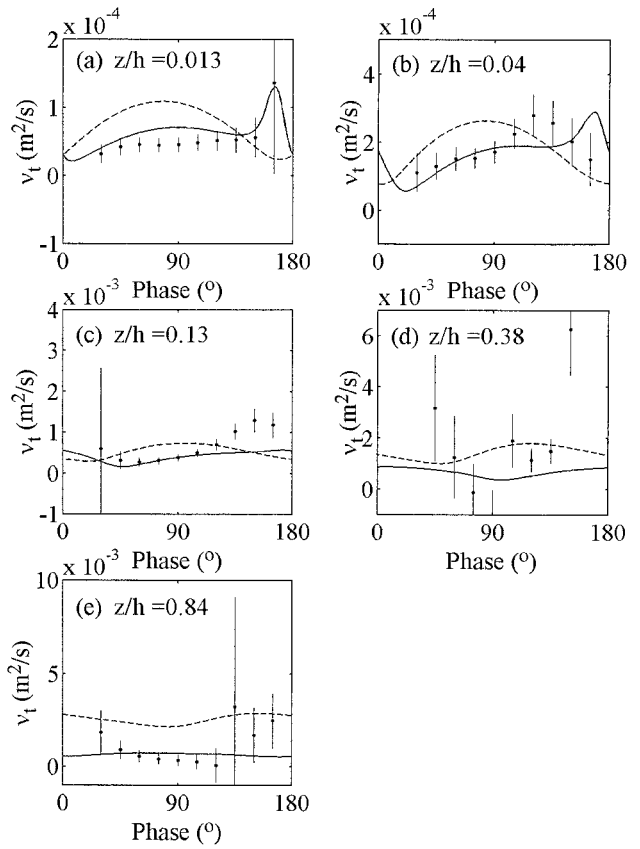

Figure 6 | Cyclic variation of eddy viscosity in comparison with Case 13 of Jensen *et al.* (1989). •Data, —— *k–ε* model, – – – *k–l* model. The vertical lines give a measure of the uncertainty in the experimental points.

and (c), the *k–ε* model returns the more satisfactory performance.

In the final series of comparisons against the data of Jensen *et al.* the sensitivity of the computations to turbulence model constants is evaluated. The value of C_μ in the *k–l* model is altered from the standard value (for that model) of 0.08 to the more familiar value of 0.09 (generally associated with the *k–ε* model). The value of 0.09 is based upon considerations of turbulence equilibrium, whereas the lower figure used in the *k–l* model may be regarded as a result of computer optimization in the context of that formulation. In terms of the *k–ε* model it is the turbulent Prandtl number for *ε*-diffusion, σ_ε, that is examined. Further assumptions related to equilibrium conditions lead to the following relation between model constants:

$$\sigma_\varepsilon = \frac{\varkappa^2}{C_\mu^{1/2}(C_{\varepsilon 2} - C_{\varepsilon 1})} \tag{18}$$

Substitution of the previously quoted standard values for the constants appearing on the right-hand side of Equation (18) gives $\sigma_\varepsilon = 1.11$, the *k–ε* model 'variant' value. Although other tests were made, here we report results for the bed shear stress in case JSF13: the maximum changes recorded in this quantity were 0.04% for the *k–l* model and 2.1% for the *k–ε* model. The sensitivity found for the *k–ε* model, where only σ_ε is altered, is modest and shows that the model performance is sufficiently 'robust' not to be strongly dependent on the precise values assigned to model coefficients. The *k–l* model test, however, has revealed what at first sight appears to be a surprising (indeed, almost total) insensitivity to the value of C_μ, a constant that is central in the formulation of the model. The reason for this finding is believed to lie in the effective boundary condition on eddy viscosity at the bed-adjacent node: combination of Equations (7) and (9) leads to the classical mixing length result:

$$(\nu_t)_{1(t)} = \varkappa U_\tau z_{1(t)} \tag{19}$$

and hence ν_t adjacent to the bed does not depend directly upon C_μ.

The UKCRF

In the remaining tests against the UKCRF and UMTF data we revert to the standard prescriptions of the *k–ε* and *k–l* models. Lloyd *et al.* (1997) conducted large-scale experiments in the UK Coastal Research Facility: while the main purpose of their published study was to examine the flow around conical islands, further data for unobstructed oscillatory flow over rough beds were also obtained. The data consist of acoustic Doppler measurements of the three components of velocity. The flow signals were recorded for six cycles of oscillation: as noted above, the sample duration is inadequate for the derivation of reliable phase-averaged data. As part of the present project, therefore, a low-pass filter was applied to the 'mean' velocity data in order to remove both noise and turbulent fluctuations from the signal (the quality of the

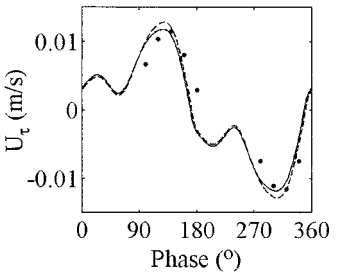

Figure 7 | Cyclic variation of friction velocity in comparison with the UKCRF data of Lloyd *et al*. (1997). •Data, —— k–ϵ model, – – – k–l model.

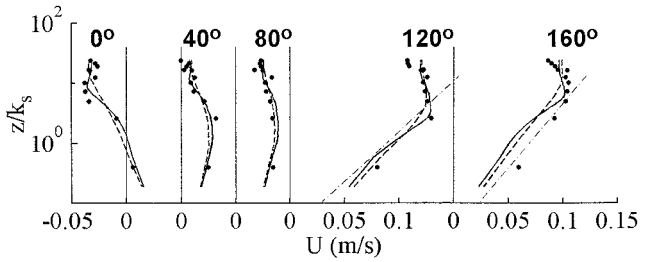

Figure 8 | Velocity profiles at various phase positions in comparison with the UKCRF data of Lloyd *et al*. (1997). •Data, —— k–ϵ model, – – – k–l model, – · – semi-logarithmic fit to data.

data did not permit any extraction of turbulence statistics). Figure 7 shows computed results for the friction velocity together with experimental points that were obtained by applying semi-logarithmic fits to the velocity profiles measured by Lloyd *et al*. The k–ε model computes the magnitude of U_τ better than the k–l model which, in common with the results for JSF12 and 13 shown in Figure 3, shows a tendency to over-predict the cycle maxima. The measured and k–ε values for $U_{\tau,\max}$ are approximately 40% above those obtained from Equation (15). It should, however, be noted that the experimentally imposed flow rate variation is not a pure sinusoid, but contains a third harmonic component. There is some evidence that both computed variations lead the data by around 10°. In Figure 8 vertical profiles of velocity are shown at five phase positions. The agreement between the two models and the data is generally acceptably close (with the exception of the lower points at the 160° phase position), although the k–ε model is seen to be the more accurate, particularly in the vicinity of the point of maximum velocity. The semi-logarithmic fits used to obtain the

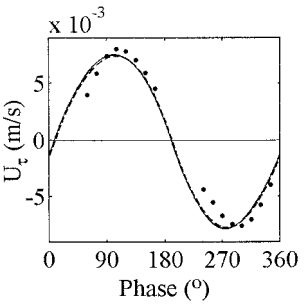

Figure 9 | Cyclic variation of friction velocity in comparison with the present UMTF data. •Data, —— k–ϵ model, – – – k–l model.

experimental values of the friction velocity are shown for the 120° and 160° phase positions.

The UMTF

The new experimental data generated in the course of the present study form part of a continuing LDA-based investigation into oscillating flows over smooth and rough beds. The UMTF is a tidal flume of dimensions 11.0 m long × 3.3 m wide × 0.2 m deep which, for the present series of experiments, was equipped with a 2-channel LDA system that permitted simultaneous measurement of the streamwise and vertical velocity components. The cyclic variation of friction velocity is shown in Figure 9 (as in the UKCRF case, the experimental points were obtained using semi-logarithmic fits to the measured velocity profiles). $U_{\tau,\max}$ as measured and also computed using the two turbulence models is approximately 8–10% lower than the value given by Equation (15). Within the reliability of the processed data, it appears that both the k–ε and k–l models lead the data by a phase margin of roughly 20°. The finding is similar to that obtained in comparison with the UKCRF friction velocity data, which were processed in a similar manner, but not in examination of the direct measurements of Jensen *et al*. (1989). Clearly then, caution must be exercised in interpreting model performance under conditions where data for an unsteady boundary layer characterized by phase shifts in the vertical direction are implicitly assumed to be quasi-steady. Velocity profiles are shown in Figure 10: at three phase positions (0°, 60°,

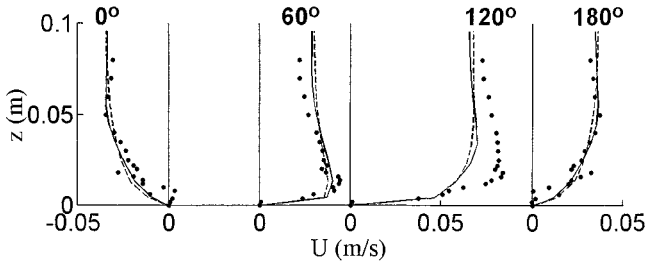

Figure 10 | Velocity profiles at various phase positions in comparison with the present UMTF data. •Data, —— k–ϵ model, – – – k–l model.

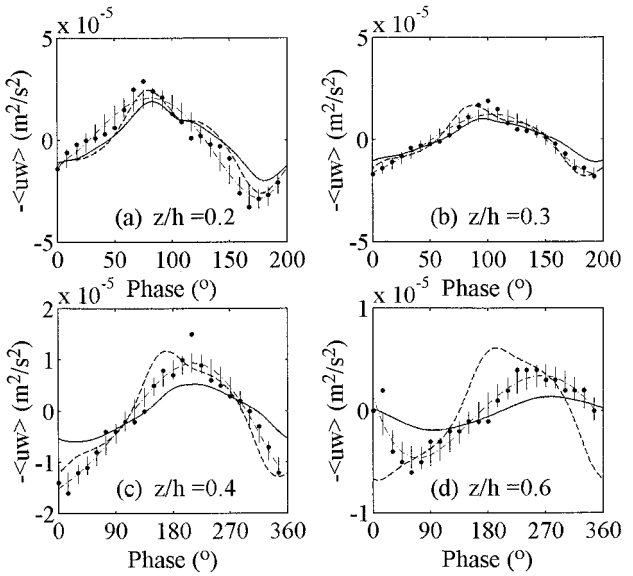

Figure 11 | Cyclic variation of Reynolds shear stress in comparison with the present UMTF data. •Data, —— k–ϵ model, – – – k–l model, – · – polynomial fit to data. The vertical lines give a measure of the uncertainty in the fit to data.

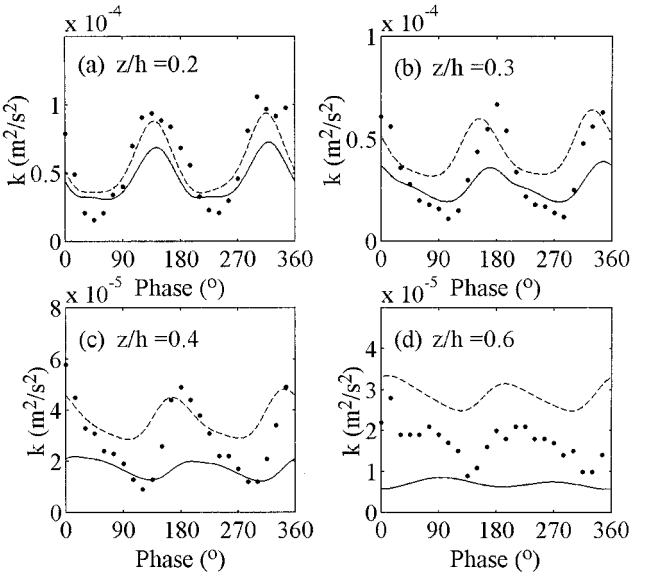

Figure 12 | Cyclic variation of turbulent kinetic energy in comparison with the present UMTF data. •Data, —— k–ϵ model, – – – k–l model. The experimental data for k are approximated by $k' = 1.3(\langle u^2 \rangle + \langle w^2 \rangle)/2$.

and 180°) the models are in acceptable agreement with the data, although the peak occurring at 120° is not resolved.

Figure 11 shows the Reynolds shear stress over one cycle of oscillation. A polynomial fit of order 5 was again made to the data (cf. case JSF13, Figure 4) and the experimental uncertainty was estimated in the same manner as before. The four elevations examined, from $z/h = 0.2$–0.6, represent moderate-to-high z/δ values (ranging from $z/\delta = 0.6$–1.7). In Figure 11(a), for which $z/\delta = 0.6$, the k–l model is somewhat more accurate than the k–ε scheme. At elevations further removed from the bed ($z/\delta = 0.86$–1.7), Figures 11(b)–(d) show that the k–ε model tends to underpredict experimental levels of Reynolds stress, whereas the k–l scheme frequently returns values that are too high. The k–ε model is consistently more accurate in resolving the phase response of the Reynolds stress field. Turbulent kinetic energy variations, with experimental data again representing k' on the basis of Svendsen's (1987) approximation, are presented in Figure 12. In Figure 12(a) the k–l model better captures the maxima (but not the minima) of the experimental turbulent kinetic energy variation. The pattern is repeated in the remaining figures for the outer flow, although it is again apparent in Figure 12(b) that the k–ε model produces the more accurate phase response.

CONCLUSIONS

k–ε and k–l turbulence models have been applied to oscillatory rough bed flows representing a wide range of defining parameters. It is found that both models predict the bed friction velocity to acceptable accuracy, although the k–ε model emerges as the superior scheme. Such capability is important in practice for general shallow

water flow modelling where the use of a friction factor correlation of the form $f_w = f_w(a/k_s)$ may be inappropriate under conditions where the boundary layer thickness, δ, is not known *a priori* (and hence δ, as well as the particle amplitude and Nikuradse roughness height, may be a relevant parameter). Velocity profiles are computed adequately by the two models. The k–ε turbulence model performs consistently better than the k–l form in terms of its ability to resolve the cyclic variations of Reynolds shear stress and turbulent kinetic energy in the lower boundary layer (roughly for $z/\delta \leq 0.1$ based upon present results). Such performance does not, however, carry over to the outer flow (the region $z/\delta \geq 0.5$) where neither model is particularly accurate in terms of computed levels of Reynolds stress or turbulent kinetic energy. Despite the failure of the k–ε model to accurately resolve the magnitude of turbulence quantities in the outer flow, it nevertheless emerges that the scheme reproduces the phase response in this region with some fidelity. Comparison with derived experimental values of eddy viscosity show the k–ε model to perform better than the k–l scheme. In relation to both Reynolds stress and eddy viscosity data, however, estimated experimental uncertainty bounds are wide and the precision with which it is possible to assess turbulence model performance is inevitably compromised to some extent.

ACKNOWLEDGEMENTS

Dr B. M. Sumer kindly provided access to the original datasets for the experiments of Jensen *et al.* (1989). SBL wishes to acknowledge the support of a UK Engineering and Physical Sciences Research Council (EPSRC) Research Studentship during the course of this study.

NOTATION

a	freestream particle amplitude
C_μ	constant in turbulence model constitutive equation
$C_{\varepsilon 1}$, $C_{\varepsilon 2}$	constants in ε-transport equation
d	grain diameter
f_w	wave friction factor
h	water depth
k	turbulent kinetic energy
k_s	Nikuradse roughness height
k_s^+	$k_s U_\tau / \nu$
l	turbulence length scale
p	pressure
Re	Reynolds number
t	time
T	period of oscillation
u,v,w	Cartesian components of fluctuating velocity
U	horizontal (phase-averaged) velocity
U_b	bulk velocity
U_∞	freestream velocity
U_0	amplitude of the freestream velocity
U_τ	friction velocity
U^+	$\mid U \mid / U_\tau$
x	horizontal coordinate
z	vertical coordinate
z^+	$z U_\tau / \nu$

Greek symbols

δ	boundary layer thickness
ε	rate of dissipation of turbulent kinetic energy
$\varkappa$	von Kármán constant
ν	molecular kinematic viscosity
ν_t	turbulent (eddy) kinematic viscosity
ρ	density
$\sigma_k, \sigma_\varepsilon$	turbulent Prandtl number for diffusion of k and ε, respectively
τ_b	bed shear stress

Subscripts

max	maximum value
1	first velocity node above the bed
1(t)	first turbulence node above the bed

REFERENCES

Baumert, H. & Radach, G. 1992 Hysteresis of turbulent kinetic energy in nonrotational tidal flows: a model study. *J. Geophys. Res.* **97** (C3), 3669–3677.

Celik, I. & Rodi, W. 1984 Simulation of free-surface effects in turbulent channel flows. *PhysicoChem. Hydrodyn.* **5**, 217–227.

Cotton, M. A. & Ismael, J. O. 1998 A strain parameter turbulence model and its application to homogeneous and thin shear flows. *Int. J. Heat Fluid Flow* **19**, 326–337.

Cotton, M. A. & Stansby, P. K. 2000 Bed frictional characteristics in a turbulent flow driven by non-linear waves. *Coastal Engng* **40**, 91–117.

Fredsøe, J. & Deigaard, R. 1992 *Mechanics of Coastal Sediment Transport*. Advanced Series on Ocean Engineering Vol. 3, World Scientific, Singapore.

Jensen, B. L., Sumer, B. M. & Fredsøe, J. 1989 Turbulent oscillatory boundary layers at high Reynolds numbers. *J. Fluid Mech.* **206**, 265–297.

Jonsson, I. G. & Carlsen, N. A. 1976 Experimental and theoretical investigations in an oscillatory turbulent boundary layer. *J. Hydraulic Res.* **14**, 45–60.

Justesen, P. 1991 A note on turbulence calculations in the wave boundary layer. *J. Hydraulic Res.* **29**, 699–711.

Letherman, S. B. 1999 k-*l* and k-*ε* modelling of oscillatory flow over rough beds. *Proc. 28th Biennial IAHR Conference, Graz* (Abstract volume, ed. M. B. Abbott *et al.*), p. 463. (Papers are available on CD-ROM.)

Lloyd, P. M., Stansby, P. K. & Chen, D. 1997 *Experiments in the UK Coastal Research Facility*. Internal Report, School of Engineering, University of Manchester.

McLean, S. R. 1983 Turbulence and sediment transport measurements in a North Sea tidal inlet (the Jade). *North Sea Dynamics* (ed. J. Sündermann & W. Lenz), pp. 436–452. Springer-Verlag, Berlin

Nezu, I. & Nakagawa, H. 1993 *Turbulence in Open-Channel Flows*. A.A. Balkema, Rotterdam.

Nielsen, P. 1992 *Coastal Bottom Boundary Layers and Sediment Transport*. Advanced Series on Ocean Engineering Vol. 4, World Scientific, Singapore.

Rodi, W. 1993 *Turbulence Models and Their Application in Hydraulics. A State-of-the-Art Review*. 3rd edn, A.A. Balkema, Rotterdam.

Sajjadi, S. G. & Waywell, M. N. 1997 Application of roughness-dependent boundary conditions to turbulent oscillatory flows. *Int. J. Heat Fluid Flow* **18**, 368–375.

Sajjadi, S. G. & Waywell, M. N. 1998 A stable algorithm for Reynolds stress turbulence modelling with applications to rectilinear and circular tidal flows. *Int. J. Numer. Meth. Fluids* **26**, 251–280.

Schlichting, H. 1979 *Boundary-Layer Theory*. 7th edn, McGraw-Hill, New York.

Schröder, M. 1987 *Messung des turbulenten Impuls- und Salztransports in der Mischungszone der Elbe*. Report GKSS 87/E/16, GKSS-Forschungszentrum Geesthacht.

Sleath, J. F. A. 1987 Turbulent oscillatory flow over rough beds. *J. Fluid Mech.* **182**, 369–409.

Stansby, P. K. 1997 Semi-implicit finite volume shallow-water flow and solute transport solver with k-*ε* turbulence model. *Int. J. Numer. Meth. Fluids* **25**, 285–313.

Sumer, B. M., Jensen, B. L. & Fredsøe, J. 1987 Turbulence in oscillatory boundary layers. *Advances in Turbulence, Proc. 1st European Turbulence Conference, Lyon* (ed. G. Comte-Bellot & J. Mathieu), pp. 556–567. Springer-Verlag, Berlin.

Svendsen, I. A. 1987 Analysis of surf zone turbulence. *J. Geophys. Res.* **92** (C5), 5115–5124.

Thais, L., Chapalain, G. & Smaoui, H. 1999 Reynolds number variation in oscillatory boundary layers. Part I. Purely oscillatory motion. *Coastal Engng* **36**, 111–146.